JOURNAL OF AIRCRAFT
Vol. 32, No. 6, November–December 1995

Aeroelastic Optimization of a Helicopter Rotor with Composite Coupling

Ranjan Ganguli* and Inderjit Chopra†
University of Maryland, College Park, Maryland 20742

Sensitivity derivatives of blade loads and aeroelastic stability of a composite helicopter rotor in forward flight are calculated as an integral part of an aeroelastic analysis using an analytical approach. Design variables are the ply angles of the laminated walls of the box–beam spar used to model the composite rotor blade. By means of a parametric study, the influence of the ply angles on the blade elastic stiffness, vibratory hub loads, and aeroelastic stability are examined for a four-bladed, soft in-plane, hingeless rotor. Aeroelastic and sensitivity analysis of the rotor, based on a finite element in space and time, are linked with an automated optimization algorithm. For the optimization, the objective function is a combination of all six vibratory hub loads and the constraints are imposed on frequency placement and aeroelastic stability in forward flight. The optimization procedure is used to tailor composite coupling for minimizing vibratory loads and enhancing aeroelastic stability of the blade in forward flight. The influence of composite coupling on the vibratory hub loads corresponding to the optimum solutions is relatively small with reductions in the objective function of about 10%. The effect of lag bending-torsion coupling in stabilizing the lag mode is significant. Starting from an initially infeasible design, the optimum design solution for a box–beam configuration with lag bending-torsion coupling shows an increase in lag damping of over 200%.

Nomenclature

C_d, C_l, C_m = blade section drag, lift, and pitching moment coefficient
C_T = rotor thrust coefficient
c = blade chord
D = section properties D_j, $j = 1, \ldots n$
EA, EI_y, EI_z, GJ = blade axial, flap, lag, and torsion stiffness
GA_y, GA_z = blade flap and lag shear stiffness
g = constraints
g_s, g_f = constraint on blade stability and frequencies
J = objective function
K^s = blade structural stiffness matrix
K_{12} = extension-lag shear coupling stiffness
K_{13} = extension-flap shear coupling stiffness
K_{14} = extension-torsion coupling stiffness
K_{25} = lag shear-flap bending coupling stiffness
K_{36} = flap shear-lag bending coupling stiffness
K_{45} = flap bending-torsion coupling stiffness
K_{46} = lag bending-torsion coupling stiffness
M^s = blade structural mass matrix
m = number of modes
m_0 = reference mass per unit length
N = number of spatial finite elements
R = rotor radius
T = kinetic energy
U = strain energy
u = axial deformation of blade
v = lag deformation of blade
W = virtual work
w = flap deformation of blade
x = normalized eigenvector of Floquet transition matrix
α = blade section angle of attack
α_k = real part of characteristic exponent of kth mode
θ = design variable (ply angle) θ_i, $i = 1, \ldots l$
λ_k = eigenvalue of kth stability mode
μ = advance ratio
σ = rotor solidity
Φ = Floquet transition matrix
ϕ = blade mode shape or eigenvector
ψ = azimuth angle, time
ψ_0 = initial azimuth angle
Ω = rotor rotational speed
ω_k = blade natural frequency of kth mode
$(\ )^L$ = lower bound
$(\ )^U$ = upper bound

Presented as Paper 92-4780 at the AIAA/USAF/NASA/OAI 4th Symposium on Multidisciplinary Analysis and Optimization, Cleveland, OH, Sept. 21–23, 1992; received Sept. 20, 1993; revision received March 30, 1995; accepted for publication May 30, 1995.

*Assistant Research Scientist, Center for Rotorcraft Education and Research, Department of Aerospace Engineering. Member AIAA.
†Professor and Director, Center for Rotorcraft Education and Research, Department of Aerospace Engineering. Fellow AIAA.

Introduction

COMPOSITE materials are widely used in the design of helicopter rotor blades because of their superior fatigue characteristics and stiffness–weight ratio, as compared to metals. There are other potential benefits of composites that need to be exploited by the rotorcraft industry, such as their flexibility in tailoring structural characteristics and cost-effective fabrication. Composite rotor designs with elastic coupling have been shown to reduce vibrations, enhance aeromechanical stability of the rotor-fuselage system, and lower blade stresses.[1–4] At this time, an extreme level of conservatism is used in the design of rotors with composites and the powerful tools of formal optimization are not exploited to tailor structural coupling to improve their performance. The objective of this research is to develop an optimization methodology

for composite rotor blades and investigate the sensitivity of structural coupling on the optimum design.

Considerable research has been done on aeroelastic optimization of helicopter rotors during the past decade.[5] Friedmann and Santhakumaran[6] applied a structural optimization procedure to reduce oscillatory hub loads (thrust or rolling moment) of a four-bladed, soft in-plane hingeless rotor. They used frequency placements and blade stability in hover as constraints. Through changes in spanwise distribution of the mass and stiffness properties of the blades, a 15–40% reduction of the vertical vibratory force was obtained.

David and Weller[7] used a modal-based optimization criteria to optimize the dynamic behavior of helicopter rotors. They also conducted two experiments to verify the analysis, first on aeromechanical stability of a bearingless rotor and the second on vibratory loads of an articulated rotor. Comparison of results from baseline and optimized configurations showed significant improvement.

Most studies on aeroelastic optimization, such as those cited previously, use finite difference methods for calculating the gradients of the objective function and constraints. Because of large computer time requirements, such studies are restrictive in terms of objective function, design variables, and constraints. This is especially true if an aeroelastic stability analysis in forward flight is included in the optimization analysis. To alleviate this problem, Celi and Friedmann[8] used a Taylor's series approximation of the objective function and constraints in terms of the design variables and an approximation technique introduced by Vanderplatts[9] to calculate the derivatives. They carried out an optimization study to minimize oscillatory vertical hub shear for a hingeless rotor with both straight and swept tip while imposing constraints on frequency placements and blade stability in hover. A reduction of 20–50% in the 4/rev vertical hub force was obtained.

Lim and Chopra[10,11] developed an efficient analytical formulation to calculate sensitivities of blade response, hub loads, and blade damping. They carried out a comprehensive study to minimize all of the vibratory hub forces and moments for helicopter rotor blades with constraints on blade stability in forward flight. Although the benefits of using analytical sensitivity analysis in structural optimization are well known, this was the first time that such an analysis was developed for a complex aeroelastic problem, with a resulting 80% reduction in CPU time to achieve the optimum solution as compared to a finite difference approach.

The need to understand the behavior of rotorcraft composite structures has led to a considerable amount of research on structural modeling of composite rotor blades over the past few years. Two approaches have emerged from this research: the finite element[12] and the direct analytical[13] approach to model composite rotor blades. While finite element methods (FEMs) are more versatile and flexible than analytical methods, they are too involved computationally. Analytical methods appear attractive to implement in a comprehensive rotor aeroelastic analysis, especially to carry out optimization studies. It is now well established that non-classical effects such as section warping, transverse shear, and in-plane elasticity become essential for the analysis of composite blades.[13] Again, these effects can be modeled in a simple way using analytical methods.

So far, few researchers have examined the impact of composite rotor blades on the rotorcraft system. It has been shown that elastic coupling induced by composite materials can have a powerful influence on aeroelastic stability, blade stresses, and loads.[1,2] These early works, however, did not precisely model the nonclassical effects. Smith and Chopra[13] addressed this limitation by extending the earlier model to include nonclassical effects. They also investigated the aeroelastic stability, hub loads, and aeromechanical stability in forward flight.[3,4]

At this time, the analytical tools needed to model the structural behavior of a composite blade are available and the research on aeroelastic optimization of metal helicopter rotors has also advanced considerably. It has now become possible to apply the powerful tools of aeroelastic optimization to explore the potential benefits of composite coupling on rotorcraft system behavior. In this article, the composite model developed by Smith and Chopra[13] is implemented in a comprehensive aeroelastic code.[14] A design-oriented analysis and optimization methodology is developed by coupling the composite rotor dynamics analysis and the design sensitivity analysis with a constrained optimization program Conmin.[15] For applications, a soft in-plane hingeless rotor with a single box–beam spar is selected. The ply angles of the laminated walls of the composite box–beams are used as the design variables. Sensitivity derivatives of blade response, rotating frequencies, hub loads, and blade stability are calculated analytically as an integral part of the aeroelastic response and stability analysis using chain-rule differentiation. The aeroelastic optimization problem consists of minimization of the 4/rev oscillatory hub loads of a 4-bladed rotor subject to frequency and stability constraints.

Any change in the design variables (the ply angles) influence both elastic stiffness and elastic coupling. Therefore, the vibration reduction obtained through the optimization process will be due to changes in both. Previous research on aeroelastic optimization of rotors has shown the effects of elastic stiffness on the optimum designs for metal blades.[5] In this article, we seek to filter out the effects of elastic coupling (obtained by tailoring composite materials) on the optimum design. For this, a baseline configuration is selected with balanced laminates. This configuration has no composite coupling and the initial optimum solution considers the effects of varying stiffness properties only. Then, aeroelastic optimizations are performed for box–beams with bending-torsion coupled layups and the optimized designs compared with the baseline design. Since the baseline design involves no coupling, the effects of elastic coupling on the final designs are isolated.

Formulation

Aeroelastic Analysis

The helicopter is modeled as elastic composite rotor blades attached to a rigid fuselage. The composite blades are modeled as slender elastic beams undergoing extension, flap and lag bending, elastic torsion, and transverse shearing deformations. The primary structural member of the blade, the blade spar, is idealized as a laminated thin-walled composite box beam. Strain displacement and stress–strain equations are developed and are used to derive the expression for the strain energy in a variational form[13]:

$$\delta U = \delta U_I(EA, GJ, EI_y, EI_z, GA_y, GA_z) + \delta U_C(K_{12}, K_{13}, K_{14}, K_{25}, K_{36}, K_{45}, K_{46}) \quad (1)$$

where δU_I is the strain energy component due to elastic stiffness and δU_C is the additional strain energy due to composite coupling. Expressions for δU for a composite rotor blade are available in Ref. 3. The kinetic energy is formulated for use in the Hamilton's principle. Since the kinetic energy is not a function of the elastic constants of the beam, it is identical for both metal and composite blades. The variational kinetic energy δT, including the shear degrees of freedom (DOF), is given in Ref. 3. External aerodynamic forces on the rotor blade contribute to the virtual work variational δW. For the aeroelastic analysis, aerodynamic forces and moments are calculated using quasisteady strip theory. Apparent mass effects are included for noncirculatory airloads. The effect of compressibility (Prandtl–Glauert correction) and reversed flow are also included in the aerodynamic model. The steady rotor inflow distribution is represented using the Drees model.[16]

Blade equations are derived using a formulation based on Hamilton's principle, and then discretized using shear flexible beam finite elements

$$\delta\Pi = \int_{\psi_1}^{\psi_2} (\delta U - \delta T - \delta W)\, dt = \int_{\psi_1}^{\psi_2} \sum_{i=1}^{N} (\delta U_i - \delta T_i - \delta W_i)\, d\psi = 0 \qquad (2)$$

Each beam element has 19 DOF (Fig. 1a) Four additional DOF (compared to existing metal rotor blade finite elements[11]) are introduced to accurately model the effects of transverse shear related deformations and couplings. These DOF correspond to cubic variations in axial elastic and (flap and lag) bending deflections, quadratic variation in elastic torsion, and linear variation in (flap and lag) transverse shear deformations.

The first step in the aeroelastic analysis procedure is to trim the vehicle for the specified operating condition. This step is important because steady loads and blade deflections can play an important role in aeroelastic stability calculations. The blade FEM equations are transformed to normal mode space for efficient solution of the blade response. The nonlinear, periodic, normal mode equations are then solved for steady response using a finite element in time method. Steady and vibratory components of the rotating frame blade loads (i.e., shear forces and bending/torsion moments) are calculated using the force summation method. In this approach, blade aerodynamic and inertia forces are integrated directly over the length of the blade. Fixed frame hub loads are calculated by summing the contributions of individual blades. A coupled trim procedure is carried out to solve for the blade response, pilot input trim controls, and vehicle orientation, simultaneously. The coupled trim procedure is essential for elastically coupled blades since elastic deflections play an important role in the steady net forces and moments generated by the rotor.

After the coupled trim solution is computed, the blade natural frequencies and mode shapes are recalculated about the (time averaged) deflected position. The blade normal mode equations are linearized about the trim position, and transformed to a system of periodic first-order differential equations. Floquet theory is applied to these differential equations to investigate blade stability. Details of the stability analysis can be found in Ref. 14.

Optimization Analysis

A general mathematical optimization problem is of the form: minimize the objective function $J(\theta)$ subject to the inequality constraints $g(\theta) \le 0$, and the move limits $\theta^L \le \theta \le \theta^U$.

For a four-bladed rotor, the objective function is a combination of the scalar norms of the 4/rev harmonics of the three forces (longitudinal, lateral, and vertical) and three moments (pitch, roll, and yaw). These forces and moments are transmitted by the rotor to the fuselage as a major source of helicopter vibration:

$$J = \sqrt{(F_{xF}^{4P})^2 + (F_{yF}^{4P})^2 + (F_{zF}^{4P})^2} + \sqrt{(M_{xF}^{4P})^2 + (M_{yF}^{4P})^2 + (M_{zF}^{4P})^2} \qquad (3)$$

The forces and moments are nondimensionalized by dividing by $m_0\Omega^2R^2$ and $m_0\Omega^2R^3$, respectively. The selection of this objective function is discussed in Ref. 10.

Ply angles of the laminated walls of the box–beam are used as design variables and are denoted by θ_i, $i = 1, \ldots, l$; where l is the number of nonzero ply angles in the layups used as design variables. It is assumed that all of the walls have the same number of plies. Depending on the nature of the layup (balanced, symmetric, or antisymmetric), the ply angles in the opposite walls may be related. In such cases, the number of design variables is reduced by explicitly reinforcing the conditions of symmetry and antisymmetry of layups.

The behavior constraints considered in this study are 1) aeroelastic stability and 2) frequency placement. The aeroelastic stability constraint keeps the rotor blade stable at a particular flight condition and is expressed as

$$g_s(\theta) = \alpha_k + \varepsilon_k \le 0, \qquad k = 1, \ldots, m \qquad (4)$$

where $\alpha_k = \sqrt{(\lambda_k^R)^2 + (\lambda_k^I)^2}/(2\pi)$ and ε_k defines the minimum acceptable level of damping for the kth mode (positive for stability). The λ_k^R and λ_k^I are the real and imaginary parts of the kth eigenvalue λ_k of the Floquet transition matrix and are calculated by solving the complex eigenvalue problem: $\lambda \boldsymbol{x} = \boldsymbol{\Phi}(\psi_0 + 2\pi, \psi_0)\boldsymbol{x}$; where $\boldsymbol{\Phi}(\psi_0 + 2\pi, \psi_0)$ is the transition matrix at the end of one rotor revolution. The frequency placement constraint prevents blade resonance at frequencies not covered by the objective function, and are expressed as $g_f^L(\theta) = 1 - \omega_k/\omega_k^L \le 0$ and $g_f^U(\theta) = 1 - \omega_k/\omega_k^U \le 0$ for the kth mode. The blade rotating natural frequency ω_k is obtained from the eigensolution of the structural equations: $\boldsymbol{K}^s\boldsymbol{\phi} = \omega_k^2\boldsymbol{M}^s\boldsymbol{\phi}$.

Sensitivity Analysis

The sensitivity derivatives of the objective function and behavior constraints are required by the optimization algorithm. Consider a general function $\boldsymbol{F}$. Differentiating $\boldsymbol{F}$ with respect to the design variable θ_k and applying the chain-rule for differentiation yields

$$\frac{d\boldsymbol{F}}{d\theta_k} = \frac{d\boldsymbol{F}}{dD_j}\frac{dD_j}{d\theta_k} = \left(\frac{\partial \boldsymbol{F}}{\partial D_j} + \frac{\partial \boldsymbol{F}}{\partial \boldsymbol{Y}}\frac{\partial \boldsymbol{Y}}{\partial D_j}\right)\frac{dD_j}{d\theta_k} \qquad (5)$$

where $D_j = \lfloor EA, GJ, EI_y, EI_z, GA_y, GA_z, K_{12}, K_{13}, K_{14}, K_{25}, K_{36}, K_{45}, K_{46} \rfloor$ are the blade section properties and $\boldsymbol{Y}$ is the blade response. Note that D_j includes all the stiffness and coupling constants contained in the virtual strain energy [Eq. (1)].[3] To calculate the sectional elastic constants D_j of the composite blade, a simple box–beam analysis is performed. The derivatives $dD_j/d\theta_k$ and $d\boldsymbol{F}/dD_j$ are calculated as an integral part of the composite box–beam analysis and the aeroelastic analysis, respectively.[17] Then using Eq. (5), the sensitivity derivatives of $\boldsymbol{F}$ with respect to θ_k are calculated. Note that the ply angle design variables cause changes in elastic stiffness and couplings, which leads to change in the blade response, and therefore, in the aerodynamic forces and moments acting on the blade. During the optimization process, the coupled trim controls are continuously updated.

Results and Discussion

For the numerical study, a four-bladed, soft in-plane hingeless composite rotor is considered. The rotor properties are given in Table 1. For the rotor aeroelastic analysis, the blade is divided into five spatial finite elements, each with 19 DOF (Fig. 1a). For discretization in the time domain, four time

Table 1 Rotor properties

Number of blades	4
Radius, ft	16.2
Hover tip speed, ft/s	650
C_l	5.73α
C_d	$0.0095 + 0.2\alpha^2$
C_m	0.0
c/R	0.08
σ	0.10
C_T/σ	0.07
Precone β_p	0.0
Lock number, γ	6.34
m_0, slug/ft	0.135

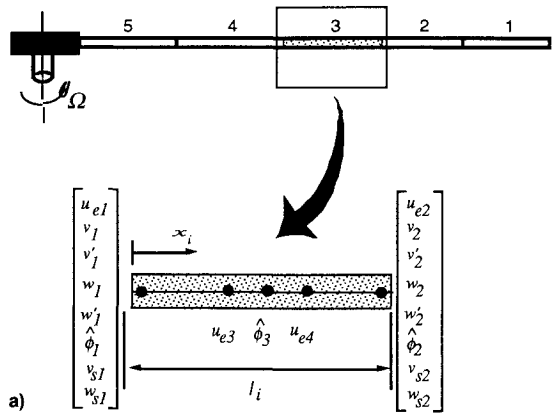

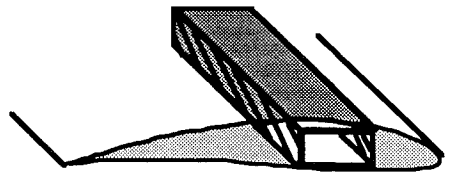
Lag bending-torsion coupling (unbalance in vertical walls)

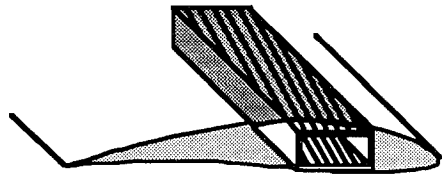
c) Flap bending-torsion coupling (unbalance in horizontal walls)

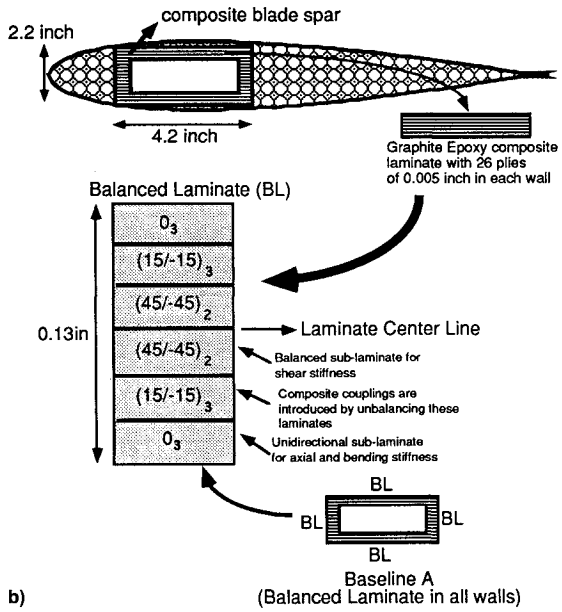

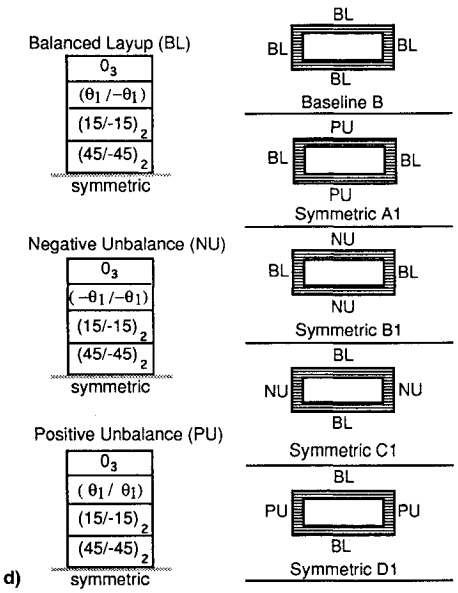

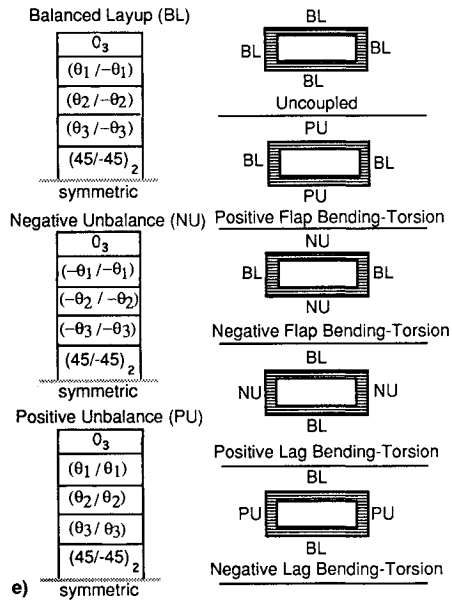

Fig. 1 a) Nineteen-degree-of-freedom shear flexible beam element used for rotor blade, b) cross-sectional dimensions and baseline laminate for the box–beam blade spar, c) spar schematic and couplings, d) composite spar laminates for different configurations (θ_1 is used for parametric study), and e) composite spar laminates for optimization study (the design variables are θ_1, θ_2, and θ_3).

finite elements with quartic polynomial distribution within each element are used. Eight normal modes (three flap, two lag, two torsion, and one axial) are used for the trim analysis and seven modes (three flap, two lag, and two torsion) are used for the stability analysis. Convergence studies show these modes to be sufficient for representing the rotor dynamics. Stability analysis is performed in the rotating frame using the Floquet transition matrix theory and the fourth-order Runge–Kutta method is used for calculating the transition matrix and its derivatives. All results are obtained for an advance ratio of 0.3 and a C_T/σ of 0.07.

The blade spar is idealized as a box–beam made of graphite epoxy (AS4/3501-6) plies. A schematic of the box–beam blade is shown in Fig. 1b. The box–beam has an outer box width of 4.2 in. and an outer box height of 2.2 in. Each wall of the box–beam has 26 plies, each having a thickness of 0.005 in. Ply elastic stiffness properties are E_L = 20.59 msi, E_T = 1.42 msi, G_{LT} = 0.87 msi, and ν_{LT} = 0.42. The ply layup of a balanced laminate is also shown in Fig. 1b. The box–beam with balanced laminates (BL) in each wall is called baseline A, and has no composite coupling. Smith and Chopra[3] formulated this box–beam configuration and the cross-sectional stiffness, inertia, and rotating natural frequencies corresponding to the blade spar are representative of a typical hingeless rotor. The $(0)_3$ sublaminates provide axial and bending stiffness and are located towards the wall edge, and the $(45/-45)_2$ sublaminates provide shear stiffness and are located near the center of the wall laminate (Fig. 1b). The $(15/-15)_3$ sublaminates are between the $(0)_3$ sublaminate and $(45/-45)_2$ sublaminate. Note that typical rotor blades have 0-deg and 45/−45-deg balanced sublaminates, with no composite coupling.

Investigation of Different Configurations

The baseline A configuration is used as a starting point in this study. Flap bending-torsion coupling K_{45} can be introduced in this layup by introducing an unbalance between the top and bottom walls of the beam, as shown schematically in Fig. 1c. Lag bending-torsion coupling K_{46} can be introduced by unbalancing the side walls of the beam (Fig. 1c). Layups showing flap bending-torsion coupling also cause K_{12} and layups with lag bending-torsion coupling cause K_{13}. Ply orientation angles used in defining these layups are positive towards the leading edge of the horizontal spar walls and positive towards the bottom of the blade section for the vertical spar walls.

To investigate the effects of varying the ply angles on the hub loads and blade stability for coupled layups, the baseline B and symmetric A1, B1, C1, and D1 cases shown in Fig. 1d are analyzed. The baseline B layup is obtained by replacing the $(15/-15)$ sublaminate adjacent to the $(0)_3$ sublaminate in baseline A (Fig. 1b), by $(\theta_1/-\theta_1)$. Next, by unbalancing the top and bottom walls of baseline B, the symmetric A1 and B1 layups are obtained. Unbalancing the side walls of the box–beams leads to the symmetric C1 and D1 layups.

The baseline B layup has no elastic coupling, the symmetric A1 and B1 layups have K_{45} and K_{12} coupling, and the symmetric C1 and D1 layups have K_{46} and K_{13}. These layups in Fig. 1d represent four types of bending-torsion coupling that can be introduced into the composite blade by changing the signs of the ply angles.

To investigate the effects of ply angles on these layups, θ_1 is varied from 0 to 90 deg. Figure 2 shows the variation of blade stiffness due to changes in θ_1. In this figure, the stiffnesses are divided by the value for the baseline B case at θ_1 = 0 deg. EI_y and EI_z display identical trends for the baseline and coupled cases at any given ply angle θ_1. The torsional stiffness shows some difference in magnitude between the baseline and coupled cases for ply angles greater than 25 deg, however, the trends are very similar.

Figures 3 and 4 show the variation in K_{45} and K_{46} for the baseline and coupled cases. The couplings are zero at angles of 0 deg, 90 deg, and θ^*. The symmetric A1 layup displays positive flap bending-torsion coupling for angles less than θ_1^* and negative flap bending-torsion coupling for angles greater than θ_1^*. At any given angle θ_1, the symmetric A1 and B1 layups show the same magnitude of coupling, but are of opposite sign. The symmetric C1 case displays positive lag bending-torsion coupling for angles below θ_1^{**} and negative lag bending-torsion coupling above θ_1^{**}. The symmetric C1 and D1 layups give the same magnitude of coupling at any given angle, but are opposite in sign. Since deflection is defined as positive for lead-lag and pitch-up motion, a positive K_{46} corresponds to a lag-back, pitch-down condition, which is negative lag bending-torsion coupling. Similarly, a negative K_{46} corresponds to positive lag bending-torsion coupling. For both flap bending-torsion and lag bending-torsion coupled layups, the maximum coupling occurs at an angle around 25 deg.

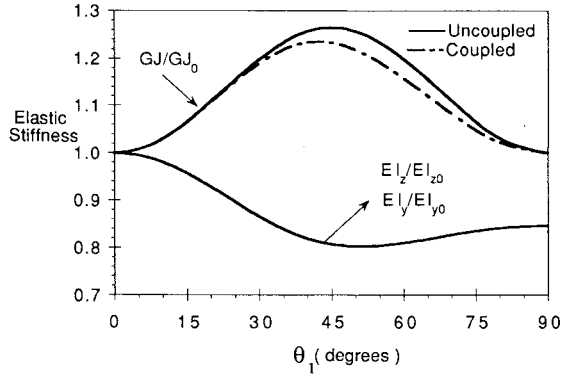

Fig. 2 Variation of flap, lag, and torsion stiffness for uncoupled and bending-torsion coupled layup.

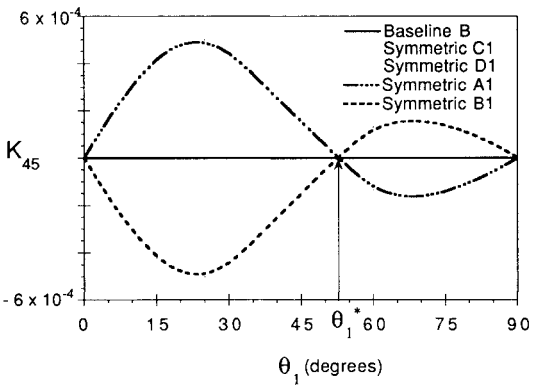

Fig. 3 Flap bending-torsion coupling.

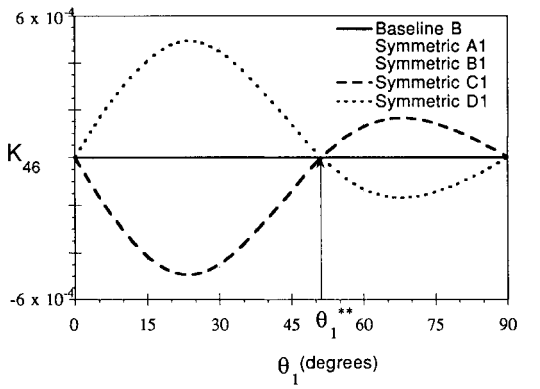

Fig. 4 Chordwise bending-torsion coupling.

The effects of variation of the ply angle θ_1 on the vibratory hub loads are shown in Figs. 5–9. In these figures, the vibratory loads are divided by the values for the baseline B case at $\theta_1 = 0$ deg. Ply angles have considerable effect on the vibratory vertical hub force, as shown in Fig. 5. However, these effects are almost entirely due to the variation of elastic stiffnesses and show very small influence of elastic coupling. The behavior of the vibratory yawing moment (not shown) is very similar to the vibratory vertical force and also shows very small influence of elastic coupling. Elastic coupling has significant influence on the vibratory longitudinal and lateral hub shear and the vibratory rolling and pitching moments. Positive lag bending-torsion coupling causes a reduction in the oscillatory longitudinal and lateral hub shear (Figs. 6 and 7). Positive flap bending-torsion coupling causes significant reduction in the oscillatory rolling moment, whereas negative coupling causes a significant increase (Fig. 8). For the oscillatory pitching moment, however, negative flap bending-torsion coupling

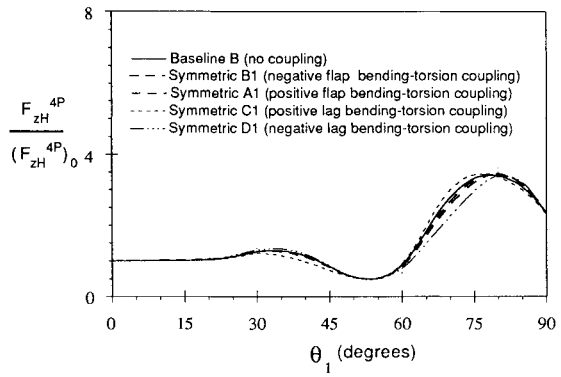

Fig. 5 Vertical 4/rev hub force for bending-torsion coupled layup.

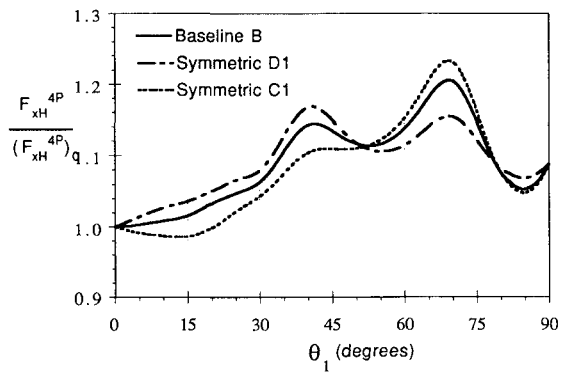

Fig. 6 Longitudinal 4/rev hub force for chordwise bending-torsion coupled layup.

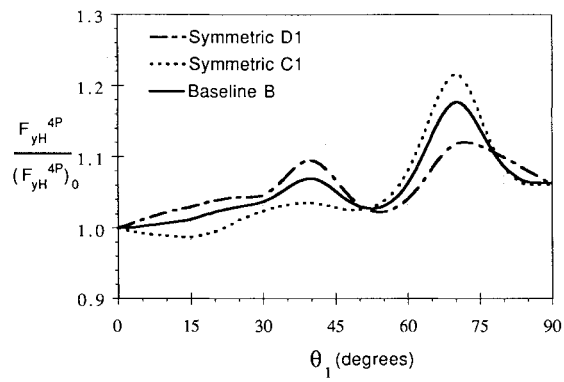

Fig. 7 Lateral 4/rev hub force for chordwise bending-torsion coupled layup.

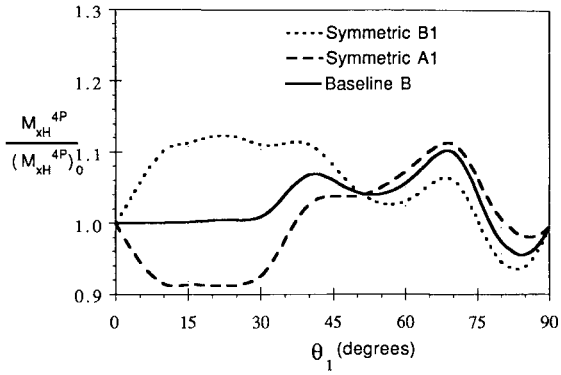

Fig. 8 Oscillatory 4/rev rolling moment for flap bending-torsion coupled layup.

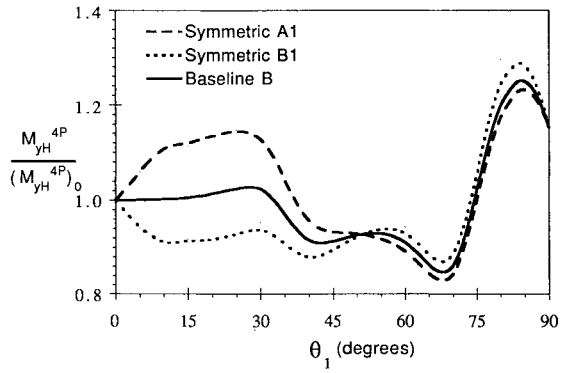

Fig. 9 Oscillatory 4/rev pitching moment for flap bending-torsion coupled layup.

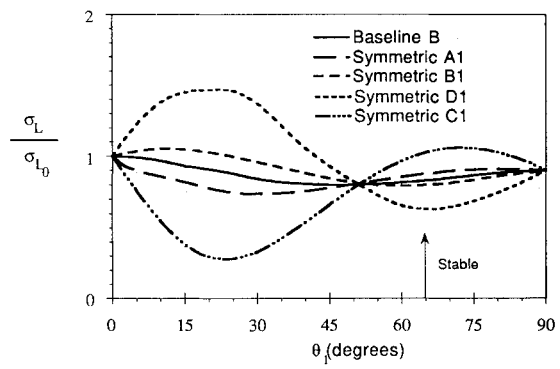

Fig. 10 Real part of lag mode eigenvalue for bending-torsion coupled layup.

is beneficial, whereas positive coupling has an adverse effect (Fig. 9).

Figure 10 shows the variation of the real part of the lag mode stability eigenvalue. In this figure, the lag mode eigenvalue is divided by the value for the baseline B case at $\theta_1 = 0$ deg. The influence of lag bending-torsion coupling on aeroelastic stability is considerably greater than the influence of flap bending-torsion coupling. Negative lag bending-torsion coupling is very stabilizing when compared to the baseline case while positive coupling is destabilizing. Negative flap bending-torsion results in a small increase in blade stability when compared to the baseline case and positive coupling results in decreased stability. The most stable configuration is obtained by the symmetric D1 layup (negative lag bending-torsion coupling), around an angle of 25 deg.

Optimization Study—Feasible Starting Design

For the optimization study, the laminates shown in Fig. 1d are modified. For example, the $(15/-15)_2$ sublaminate in

baseline B (Fig. 1d) is replaced by the $(\theta_2/-\theta_2)(\theta_3/-\theta_3)$ sublaminate in the uncoupled layup in Fig. 1e. The other laminates used for the optimization study are obtained by unbalancing the uncoupled layup and are also shown in Fig. 1e. The angles θ_1, θ_2, and θ_3 are the design variables. This choice of design variables is motivated by the design study conducted earlier. For example, in Figs. 2–4, varying θ_1 resulted in changes in the elastic stiffnesses of about 20–25% and also resulted in a considerable amount of coupling. Considering the relatively large changes in the elastic properties brought about by varying only θ_1 for the layups in Fig. 1d, three ply angles θ_1, θ_2, and θ_3 are considered to be sufficient for improving system characteristics using optimization. The five cases in Fig. 1e are labeled as uncoupled, positive flap bending-torsion, negative flap bending-torsion, positive lag bending-torsion, and negative lag bending-torsion, depending on the type of coupling associated with each layup.

These design variables, however, effect 12 plies in each wall, and hence, a total of 48 plies for all four walls of the box–beam. Each wall of the box–beam has 26 plies, which implies a total of 104 plies for the box–beam. The 0- and 45-deg plies are retained to assure that the designs do not become unrealistic. In this way, implicit move limits are applied on the values of the elastic stiffnesses and coupling. Therefore, ply angles of 48 plies undergo change during the optimization process while the remaining 56 plies undergo no change in their orientations. Move limits are explicitly imposed on the ply angles. The allowable movement of the ply angle design variable is limited by $\theta^L = \theta_{i-1} - 15(0.9)^{i-1}$, and $\theta^U = \theta_{i-1} + 15(0.9)^{i-1}$, where θ^L and θ^U are the lower and upper bounds placed on θ, and i is the iteration number. The previous equations are suggested by Watkins and Morris[18] as being good for numerical stability and convergence.

The optimization is performed to minimize the objective function J defined by Eq. (3). The upper and lower bounds on the blade frequencies are $0.60/\text{rev} \leq \omega_{1L} \leq 0.80/\text{rev}$, $1.08/\text{rev} \leq \omega_{1F} \leq 1.18/\text{rev}$, and $2.50/\text{rev} \leq \omega_{1T} \leq 6.50/\text{rev}$, where the subscripts $1L$, $1F$, and $1T$ denote the first lag, flap, and torsion modes, respectively. For the stability constraint ε_k [see Eq. (4)] is chosen to be zero. This implies that the rotor is assumed to become unstable when the damping of any of the stability modes becomes negative.

To investigate the effects of individual coupling on the optimum design, the optimization is performed with several different layups shown in Fig. 1e. The optimization of the uncoupled layup is started from $\theta_1 = 15$ deg, $\theta_2 = 30$ deg, and $\theta_3 = 15$ deg. This starting design is feasible (satisfies all the constraints and move limits) and the optimizer shows good convergence characteristics when starting from this design. The objective function J is reduced by about 40% relative to the starting design, as shown in Fig. 11. The vibratory hub

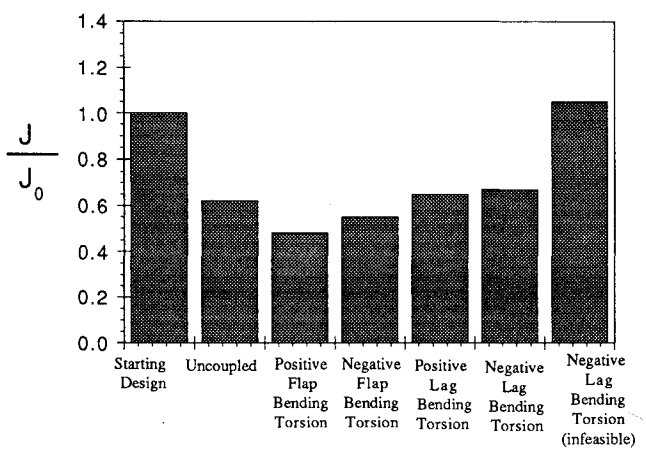

Fig. 11 Objective function corresponding to initial and optimum designs.

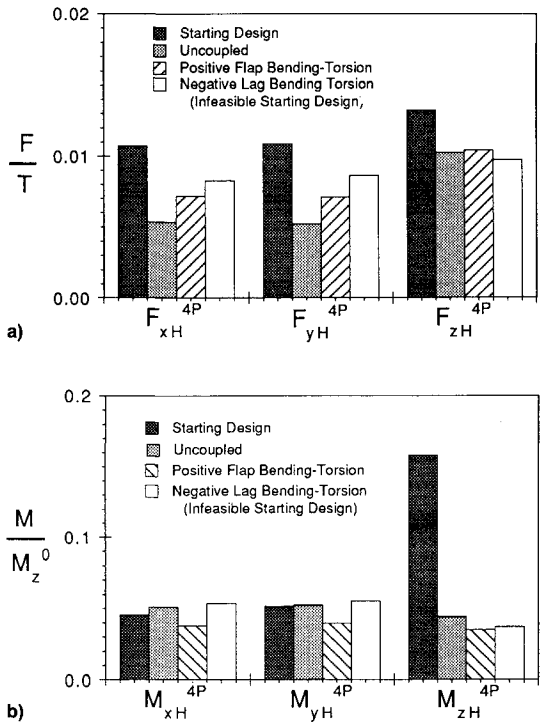

Fig. 12 a) Vibratory hub forces corresponding to initial and optimum designs nondimensionalized by steady rotor thrust and b) vibratory hub moments corresponding to initial and optimum designs nondimensionalized by steady rotor yawing moment.

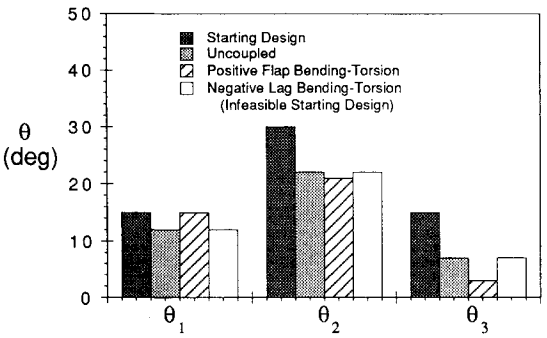

Fig. 13 Design variables corresponding to initial and optimum designs.

forces and moments corresponding to the optimum designs of several different layups are shown in Figs. 12a and 12b, respectively. For the uncoupled layup, there is a reduction in all of the vibratory hub forces and, in fact, there is a dramatic reduction of nearly 70% in the vibratory yawing moment. Since the uncoupled layup displays no elastic couplings, this reduction in the vibratory loads is due to change in the elastic stiffnesses only. The optimum angles are obtained as $\theta_1 = 12$ deg, $\theta_2 = 22$ deg, and $\theta_3 = 7$ deg, where the angles were rounded up to the nearest integer value (Fig. 13). As shown in Fig. 14, the flap and lag frequencies are almost unchanged, however, the torsion frequency decreases from 4.82 to 4.61 (a 4.3% reduction) from the starting design to the uncoupled optimum design. There is an increase in the lag mode damping of about 45%, as shown in Fig. 15. The trim control angles in Fig. 16 show small change between the starting design and the uncoupled optimum design. The results shown in Figs. 11–16 for the starting design, uncoupled and positive flap bending-torsion, and negative lag bending-torsion layups, are obtained by running the aeroelastic code after the optimum design angles have been rounded to the nearest integer. The results for the positive flap bending-torsion and negative lag

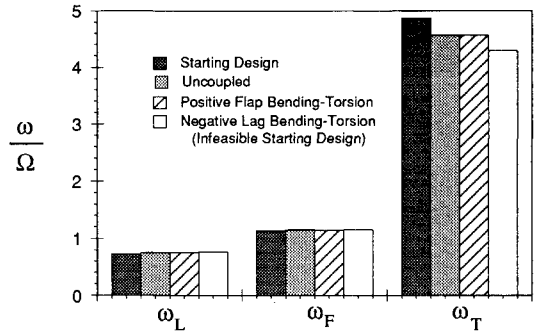

Fig. 14 Blade rotating frequencies corresponding to initial and optimum designs.

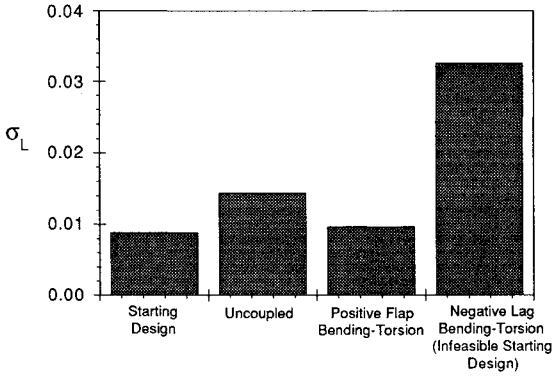

Fig. 15 Blade lag mode damping corresponding to initial and optimum designs.

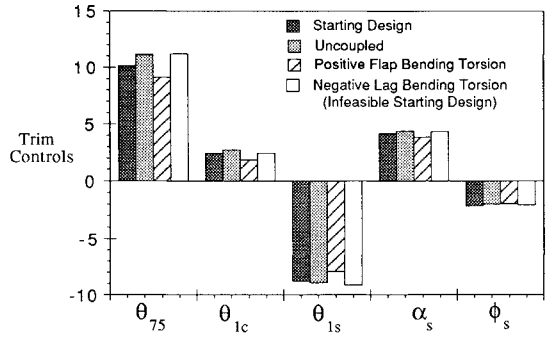

Fig. 16 Trim control angles corresponding to initial and optimum designs.

bending-torsion (infeasible starting design) cases are discussed next.

The optimum design angles for the uncoupled layup are used as the initial case for performing optimization on the four coupled layups. The positive flap bending-torsion layup shows a further reduction in the objective function of about 10% from the uncoupled optimum design (Fig. 11). The optimum angles are shown in Fig. 13 as $\theta_1 = 15$ deg, $\theta_2 = 22$ deg, and $\theta_3 = 3$ deg. There is almost no change in the blade frequencies between the uncoupled optimum and the flap bending-torsion coupling optimum (Fig. 14). The lag mode damping, however, decreases by about 34%, compared to the uncoupled optimum (Fig. 15). Again, the change in trim controls is small, as shown in Fig. 16.

The positive lag bending-torsion layup shows a reduction in the objective function of about 5% (Fig. 11). The negative flap bending-torsion and negative lag bending-torsion layups show no reduction in the objective function.

Optimization Study—Infeasible Starting Design

During the optimization iterations, neither the stability nor the frequency constraints were violated. From earlier results, it is clear that since elastic couplings have a small influence on vibratory hub loads and a larger influence on blade stability, their effect on the optimum solution is small. It may be noted from the design study conducted earlier that the symmetric B1 and D1 cases (negative flap bending-torsion and lag bending-torsion coupling, respectively) showed increases in the vibratory loads compared to the baseline case, but significantly stabilized the blade. During the optimization process, the stability constraint was never violated, and therefore, the beneficial effects of coupling on the aeroelastic stability were not exploited. The negative flap bending-torsion and negative lag bending-torsion layups, therefore, did not move from the starting design, since any move would have resulted in an increase in the objective function. It is possible that these cases could give beneficial results with marginally stable or unstable starting designs.

In order to make the stability constraint active during the design process, a margin of 3% blade damping is imposed, which makes all the previous designs infeasible. The optimization process is then performed for all the layups in Fig. 1e and the angles from the uncoupled optimum layup (now an infeasible design) are used as a starting point. Only the negative lag bending-torsion layup achieves a feasible design. For the remaining layups, the optimizer is unable to move the design into the feasible region. The negative lag bending-torsion case shows a rise in the objective function compared to the uncoupled optimum of about 45% (Fig. 11) and an increase in lag mode damping of about 130% (Fig. 15). Compared to the starting design, the objective function increases by about 5% and the lag mode damping by over 200%. The optimum solution is $\theta_1 = 7$ deg, $\theta_2 = 12$ deg, and $\theta_3 = 6$ deg (Fig. 13). The torsion frequency of the negative lag bending-torsion optimum design is reduced by 7.5% compared to the starting design (Fig. 14), however, the flap and lag frequencies are almost unchanged. Also, the change in trim controls is small (Fig. 16).

The previous results show that, among the coupled layups, the positive flap bending-torsion case shows maximum reduction in the vibratory loads (about 10%) and the negative lag bending-torsion case shows maximum increase in blade stability (about 130%) compared to the baseline optimum design. Compared to the starting design, however, the reduction in the objective function is about 50% and the increase in lag damping is over 200%, due to the combined effects of composite couplings and elastic stiffnesses. Therefore, from the standpoint of vibration reduction, positive flap bending-torsion coupling yields the best design and from the standpoint of increase in lag mode damping, negative lag bending-torsion coupling yields the best design.

The previous results were obtained with quasisteady aerodynamics. However, results obtained by performing the aeroelastic analysis with a free-wake inflow model[19] and unsteady aerodynamics[20] also show a reduction in the objective function at several forward speeds, even though the optimum

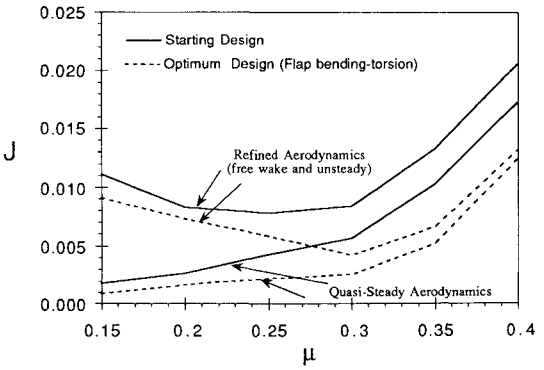

Fig. 17 Variation of objective function with forward speed (design condition is quasisteady aerodynamics and $\mu = 0.3$).

design was obtained with a quasisteady aerodynamic model at an advance ratio of $\mu = 0.3$ (Fig. 17).

Conclusions

Using an analytical formulation, rotor sensitivity analysis is developed for a composite blade. Shear effects are modeled using shear flexible finite elements. For the numerical study, a four-bladed, soft in-plane hingeless rotor is investigated. The optimization problem consists of minimizing the objective function consisting of 4/rev hub loads, with constraints on frequency placement and aeroelastic stability in forward flight. The composite blade spar is idealized as a box–beam. Design variables are the ply angles of the box–beam walls. The following conclusions are drawn from this study:

1) Significant changes in the elastic stiffnesses and coupling of the composite rotor blade can be obtained by varying a few ply angles in the walls of the box–beam blade spar.

2) Compared to the starting design, a reduction of about 40% is obtained in the objective function due to the effects of elastic stiffnesses only. Positive flap bending-torsion coupling yields an additional reduction of about 10%. Therefore, elastic stiffness and composite couplings together can yield vibration reduction of almost 50%.

3) Starting with an initially feasible design with a stability margin of 3% in the lag mode, a coupled layup with negative lag bending-torsion coupling results in an increase in the lag mode damping of over 200%, compared to the starting design. This increase in lag damping comes at the expense of an increase in the objective function of about 5%.

4) The aeroelastic optimization is performed using quasisteady aerodynamic modeling at $\mu = 0.3$. With the inclusion of free wake and unsteady aerodynamic models, the optimum design shows reductions in the objective function in comparison to the quasisteady results, at the design condition ($\mu = 0.3$), as well as at off-design conditions. In fact, the beneficial effects of composite coupling and stiffnesses on vibration reduction are enhanced at higher forward speeds.

Acknowledgments

This research was supported by the Army Research Office, Contract DAAL-03-99-C0002; technical monitors were Robert Singleton and Tom Doligalski.

References

[1]Hong, C. H., and Chopra, I., "Aeroelastic Stability of a Composite Blade," *Journal of the American Helicopter Society*, Vol. 30, No. 2, 1985, pp. 29–35.

[2]Panda, B., and Chopra, I., "Dynamics of Composite Rotor Blades in Forward Flight," *Vertica*, Vol. 11, Nos. 1–2, 1987, pp. 107–209.

[3]Smith, E. C., and Chopra, I., "Aeroelastic Response, Loads and Stability of a Composite Rotor in Forward Flight," *AIAA Journal*, Vol. 31, No. 7, 1993, pp. 1265–1274.

[4]Smith, E. C., and Chopra, I., "Air and Ground Resonance of Helicopters with Elastically Tailored Composite Rotor Blades," *Journal of the American Helicopter Society*, Vol. 38, No. 4, 1993, pp. 50–61.

[5]Friedmann, P. P., "Helicopter Vibration Optimization Using Structural Optimization with Aeroelastic/Multidisciplinary Constraints," *Journal of Aircraft*, Vol. 28, No. 1, 1991, pp. 8–21.

[6]Friedmann, P. P., and Santhakumaran, P., "Aeroelastic Tailoring of Rotor Blades for Vibration Reduction in Forward Flight," *Journal of the American Helicopter Society*, Vol. 29, No. 4, 1984, pp. 70–80.

[7]Davis, M. W., and Weller, W. H., "Helicopter Rotor Dynamics Optimization with Experimental Verification," *Journal of Aircraft*, Vol. 28, No. 1, 1991, pp. 38–48.

[8]Celi, R., and Friedmann, P. P., "Structural Optimization with Aeroelastic Constraints of Rotor Blades with Straight and Swept Tips," *AIAA Journal*, Vol. 28, No. 5, 1990, pp. 928–936.

[9]Vanderplatts, G. N., "Approximation Concepts for Numerical Airfoil Optimization," NASA TP-1370, March 1979.

[10]Lim, J., and Chopra, I., "Aeroelastic Optimization of a Helicopter Rotor," *Journal of the American Helicopter Society*, Vol. 34, No. 1, 1989, pp. 55–62.

[11]Lim, J., and Chopra, I., "Aeroelastic Optimization of a Helicopter Rotor Using an Efficient Sensitivity Analysis," *Journal of Aircraft*, Vol. 28, No. 1, 1991, pp. 29–37.

[12]Kosmatka, J. B., and Friedmann, P. P., "Vibration Analysis of Composite Turbopropellers Using a Nonlinear Beam-Type Finite Element Approach," *AIAA Journal*, Vol. 27, No. 11, 1989, pp. 1606–1614.

[13]Smith, E. C., and Chopra, I., "Formulation and Evaluation of an Analytical Model for Composite Box Beams," *Journal of the American Helicopter Society*, Vol. 36, No. 3, 1991, pp. 23–35.

[14]Bir, G., Chopra, I., and Nguyen, K., "Development of UMARC (University of Maryland Advanced Rotor Code)," *Proceedings of the 46th Annual National Forum of the American Helicopter Society* (Washington, DC), American Helicopter Society, 1990, pp. 55–70.

[15]Vanderplatts, G. N., "CONMIN—A Fortran Program for Constrained Function Minimization," *User's Guide*, NASA TMX 62282, Aug. 1973.

[16]Johnson, W., *Helicopter Theory*, Princeton Univ. Press, Princeton, NJ, 1980, pp. 139–141.

[17]Ganguli, R., and Chopra, I., "Aeroelastic Optimization of a Composite Helicopter Rotor," AIAA Paper 92-4780, Sept. 1992.

[18]Watkins, R. I., and Morris, A. J., "A Multicriteria Objective Function Optimization Scheme for Laminated Composites for Use in Multilevel Structural Optimization Schemes," *Computational Methods for Applied Mechanical Engineering.*, Vol. 60, No. 1, 1987, pp. 233–251.

[19]Scully, M. P., "Computation of Helicopter Rotor Wake Geometry and Its Influence on Rotor Harmonic Airloads," Massachusetts Inst. of Technology, ASRL TR 178-1, Cambridge, MA, March 1975.

[20]Leishman, J. G., and Beddoes, T. S., "A Generalized Model for Unsteady Aerodynamic Behavior and Dynamic Stall Using the Indicial Method," *Proceedings of the 42nd Annual Forum of the American Helicopter Society* (Washington, DC), American Helicopter Society, 1986, pp. 243–265.